University of Groningen

Identification and Characterization of a Small Molecule that Activates Thiosulfate Sulfurtransferase and Stimulates Mitochondrial Respiration

Al-Dahmani, Zayana M; Hadian, Mojgan; Ruiz-Moreno, Angel J; Maria, Sabogal-Guaqueta Angelica; Batista, Fernando A; Zhang, Ran; Luo, Yang; Sadremomtaz, Afsaneh; van der Straat, Robin; Spoor, Mette

IMPORTANT NOTE: You are advised to consult the publisher's version (publisher's PDF) if you wish to cite from it. Please check the document version below.

Document Version
Publisher's PDF, also known as Version of record

Publication date:
2023

Link to publication in University of Groningen/UMCG research database

bio-techne®

Accelerating Protein Analysis Throughput at Boehringer Ingelheim

Thank you for your interest in our webinar!
You can now view on-demand via the link below.

Watch Now
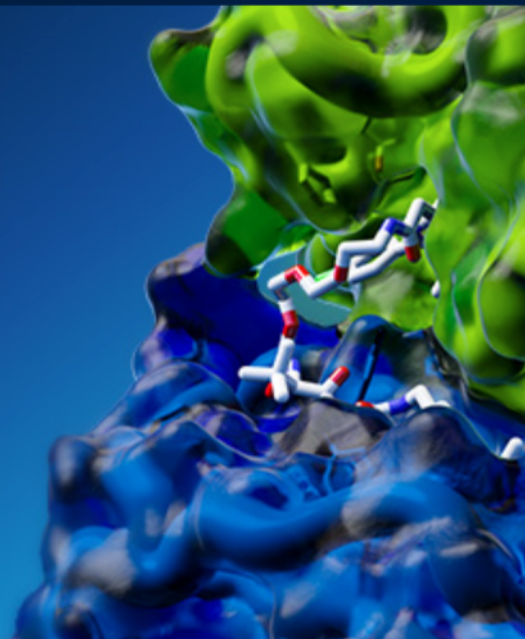
Reducing the Bottleneck of Quantitative Protein Analysis in Targeted Protein Degradation Research

Watch on-demand as Andrea Stingu, Johannes Wachter and Teresa Puchner from Boehringer Ingelheim present their TPD research on the Simple Western platform. In this webinar, our speakers...

- Delve into two real-world project instances featuring in-depth data analysis, and highlight the challenges overcome.
- Share insights into efficient device and consumable management strategies.
- Explore the application of Simple Western and optimized assay setups, backed by an impressive 15,688 runs conducted by the team to date.

Speakers

Andrea Stingu
Lab Scientist
Boehringer Ingelheim

Johannes Wachter
Lab Scientist
Boehringer Ingelheim

Teresa Puchner
Lab Scientist
Boehringer Ingelheim

View On-Demand

RESEARCH ARTICLE

THE PROTEIN SOCIETY WILEY

Identification and characterization of a small molecule that activates thiosulfate sulfurtransferase and stimulates mitochondrial respiration

Zeyana M. Al-Dahmani[1,2] | Mojgan Hadian[1] | Angel J. Ruiz-Moreno[1] |
Sabogal-Guaqueta Angelica Maria[3] | Fernando A. Batista[1,4] | Ran Zhang[1] |
Yang Luo[2,3] | Afsaneh Sadremomtaz[1,5,6] | Robin van der Straat[1] |
Mette Spoor[1] | Amalia M. Dolga[3] | Frank J. Dekker[7] |
Alexander Dömling S S[1] | Harry van Goor[2] | Matthew R. Groves[1]

[1]Department of Pharmacy and Drug Design, University of Groningen, Groningen, The Netherlands

[2]Department of Pathology and Medical Biology, University Medical Center Groningen, Groningen, The Netherlands

[3]Department of Pharmacy, Molecular Pharmacology, University of Groningen, Groningen, The Netherlands

[4]Department of Microbiology Structure, Institute of Pasteur, Paris, France

[5]Department of Nanoengineering, University of North Carolina Agriculture and Technical State, Greensboro, North Carolina, USA

[6]Department of Nanoengineering, Joint School of Nanoscience and Nanoengineering, Greensboro, North Carolina, USA

[7]Department of Pharmaceutical Gene Modulation, University of Groningen, Groningen, The Netherlands

Correspondence
Harry van Goor, Universitair Medisch Centrum Groningen Pathologie en Medische Biologie, Groningen, 9700 RB, The Netherlands.
Email: h.van.goor@umcg.nl

Abstract

The enzyme Thiosulfate sulfurtransferase (TST, EC 2.8.1.1), is a positive genetic predictor of diabetes type 2 and obesity. As increased TST activity protects against the development of diabetic symptoms in mice, an activating compound for TST may provide therapeutic benefits in diabetes and obesity. We identified a small molecule activator of human TST through screening of an inhouse small molecule library. Kinetic studies in vitro suggest that two distinct isomers of the compound are required for full activation as well as an allosteric mode of activation. Additionally, we studied the effect of TST protein and the activator on TST activity through mitochondrial respiration. Molecular docking and molecular dynamics (MD) approaches supports an allosteric site for the binding of the activator, which is supported by the lack of activation in the *Escherichia coli.* mercaptopyruvate sulfurtransferase. Finally, we show that increasing TST activity in isolated mitochondria increases mitochondrial oxygen consumption.

Reviewing Editor: John Kuriyan

Matthew R. Groves and Harry van Goor are both senior authors.

----

1 | INTRODUCTION

Thiosulfate sulfurtransferase (TST, EC 2.8.1.1), also known as rhodanese, is a mitochondrial enzyme present in both prokaryotes and eukaryotes. TST has been found in a variety of animal tissues, and its distribution pattern appears to be highly species and tissue specific (Billaut-Laden et al., 2006). It is also distributed widely in plants and in large amounts in human liver tissue (Aminlari et al., 2007; Selles et al., 2007). TST is synthesized on free cytosolic ribosomes and then imported into mitochondria (Miller et al., 1991; Smirnov et al., 2010). In 1933, TST's enzymatic activity was found to be essential for cyanide detoxification. It was shown that sodium thiosulfate might be used as a sulfur donor in TST catalyzed cyanide sulfonation (Kruithof et al., 2020). The enzyme has now been used in toxicology for decades to treat cyanide poisoning in humans and to detect and quantify cyanide levels in the blood (Kruithof et al., 2020; Sylvester & Sander, 1990) and enhanced TST activity may improve the efficiency of these approaches. It is also involved in other processes such as Fe/S cluster formation, and redox reactions as well as intracellular transport and regulatory mechanisms (Kruithof et al., 2020; Smirnov et al., 2010).

Diabetes mellitus is a severe health condition that has spread across geographical and genetic boundaries. Obesity represents a risk factor for the evolution of insulin resistance and, as a result, overt type 2 diabetes—as seen by the rising incidence of type 2 diabetes combined with rising obesity (Rao et al., 2008). Obese people have hyperinsulinemia, which correlates with the degree of insulin resistance to maintain appropriate glucose tolerance in both normoglycemic and hyperglycemic conditions (Bonadonna et al., 1990; Rao et al., 2008). The progressive degradation of the metabolic milieu after reaching a certain point leads to the failure of hyperinsulinemia to adequately compensate for insulin resistance, resulting in impaired glucose tolerance that leads to diabetes (Hales, 1994; Rao et al., 2008). Treatment of diabetic mice with thiosulfate, the major substrate for TST improved their glucose-uptake and reversed the effects of insulin resistance on 3T3-L1 adipocytes (Kruithof et al., 2020; Morton et al., 2016). However, TST overexpression further improved these effects (Morton et al., 2016), suggesting that a TST activator might have clinical benefit (Al-Dahmani et al., 2022; Kruithof et al., 2020).

We screened 623 compounds of our in-house synthesized library of small molecules, identified a small molecule activator of TST, and established and measured the link between TST activity and mitochondrial respiratory function. For this, we adopted the following strategy: first, human TST (*h*TST) was recombinantly expressed in *Escherichia coli* (*E. coli*), a purification protocol was established and the cyanide detoxification activity of TST was measured in vitro (Libiad et al., 2018; Sörbo et al., 1953). The sulfurtransferase activity of TST was measured in the presence of compounds of the in-house library. From the compounds that were found to have an activating effect in vitro, the best were selected to be tested for their potential effect on mitochondrial respiration using the high-resolution respirometry Oroboros method. As the initial hit compound possess two distinct stereocenters we isolated the individual stereoisomers and demonstrated that while individual isomers possess activation properties, optimal activation is provided by a mix of distinct stereoisomers. Enzyme kinetic investigations also indicated that the TST activator binds to an allosteric binding site on *h*TST and it is not competitive with the substrates—in agreement with in silico modeling studies. A model of *h*TST was created using the available highly homologous bovine TST (*b*TST) structure (Kruithof et al., 2020). This model was used to predict the binding of our identified compound with *E. coli* mercaptopyruvate sulfurtransferase (*ec*MST) and *b*TST and the ability of this compound to activate these homologs was determined. Whereas, activation of *b*TST could be shown, no activation of *ec*MST could be seen under identical conditions. Given the high degree of sequence conservation within the active site of these enzymes with *h*TST, this data further support an allosteric and species selective activation mechanism.

2 | RESULTS

2.1 | Screening of the fragment library

Initial screening was performed to identify activators of the reaction catalyzed by *h*TST. The activator screening resulted in the identification of 14 compounds as shown in Figure 1a.

2.2 | Differential scanning fluorimetry (DSF)

The 14 different compounds identified above were screened using differential scanning fluorimetry in triplicate to identify those that interact directly with *h*TST. Of
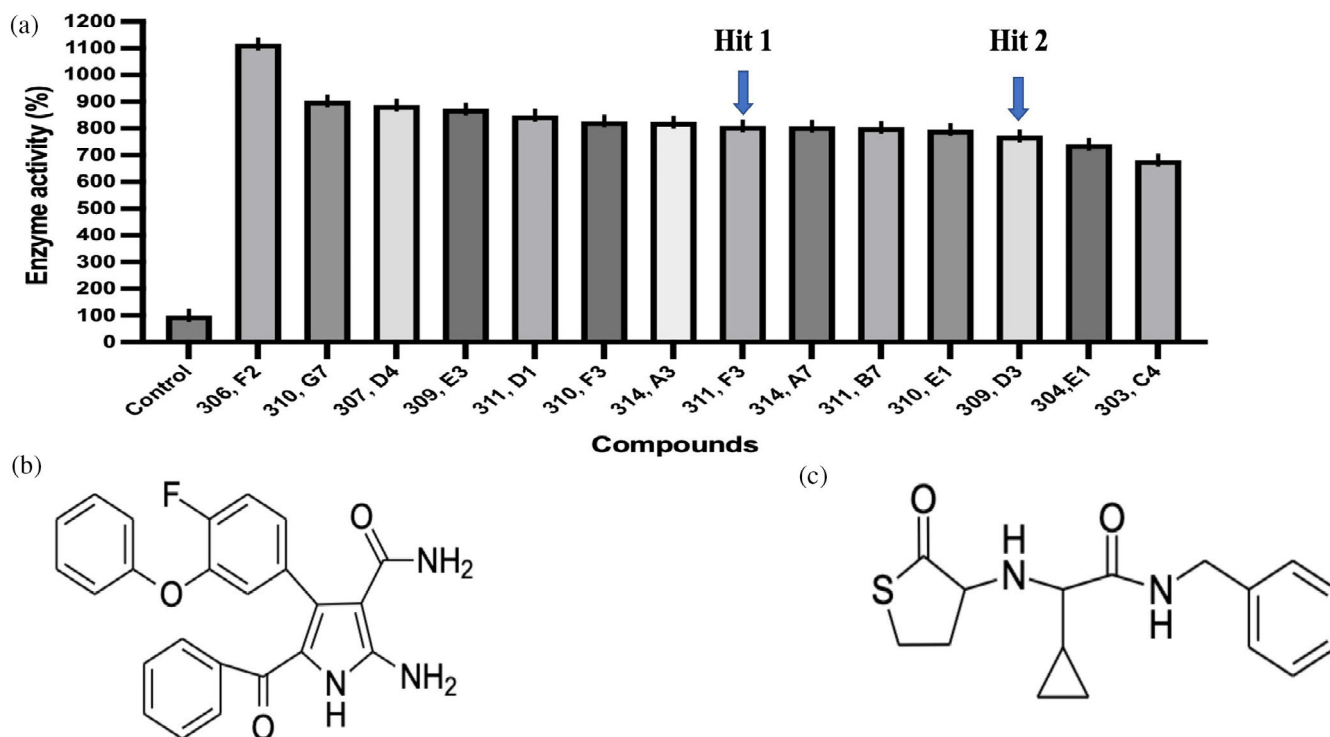
FIGURE 1 (a) Activity of TST in the presence of 1 mM test compound as a percentage of base activity. (b) Chemical structure of **Hit 1**. (c) Chemical structure of **Hit 2**.
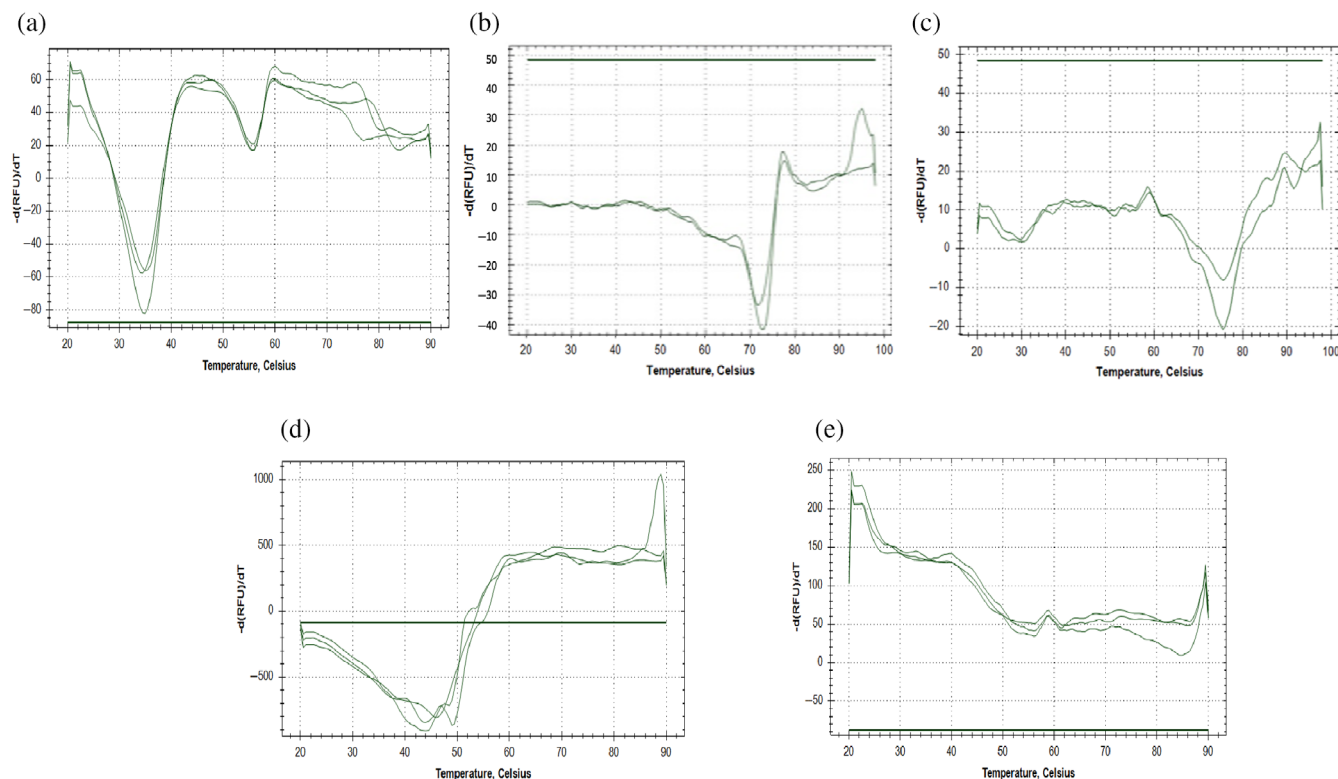
FIGURE 2 (a) DSF screening result of TST without compound. This curve was used as a reference to judge the TST stabilizing ability of the potential activators that were screened. (b) DSF results when testing the stability of TST in presence of **Hit 1**. The melting point was increased to 72°C. (c) DSF results when testing the stability of TST in presence of **Hit 2**. The melting point was increased to 76°C. (d) DSF results of **HIT 1** without protein. (e) DSF results of **HIT 2** without protein.
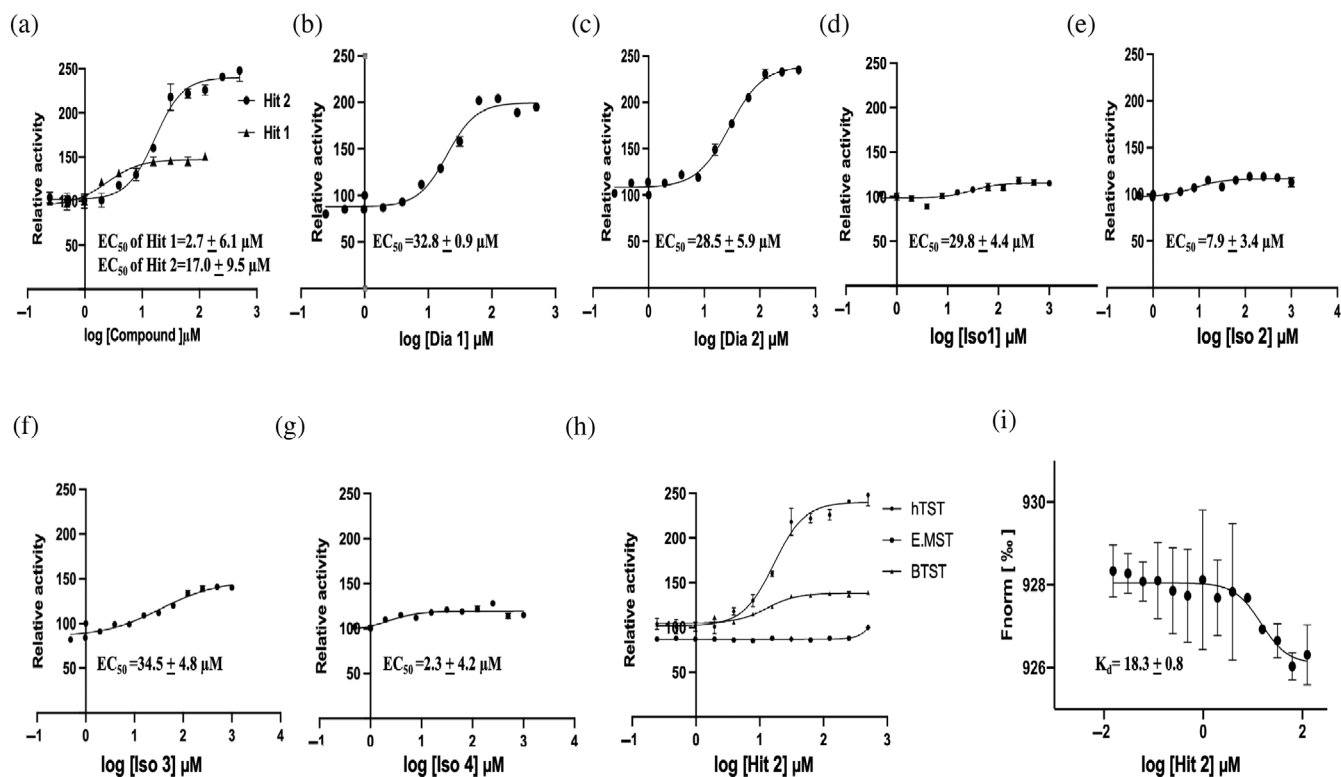
FIGURE 4 (a) Activity assay of hTST with **Hit 1** and **Hit 2** at concentrations from 0.244 to 500 μM. (b, c) Activity assay of hTST with **Dia 1** and **Dia 2**, at concentrations from 0.244 to 500 μM. (d–g) Activity assay of hTST with **Iso1**, **Iso 2**, **Iso 3**, and **Iso 4** at concentrations from 0.244 to 500 μM. (h) Activity assay of **Hit 2** with hTST, bTST, and ecMST at concentrations from 0.244 to 500 μM. (i) MST binding assay of hTST to **Hit 2**. The concentration-response curve showed the interaction between the RED-tris-NTA dye labeled hTST and **Hit 2**, each measurement was performed in triplicate. F_{norm}, normalized fluorescence.

these compounds, 2 were shown to increase the stability of hTST, suggesting a direct physical interaction between the compound and hTST: **Hit1** and **Hit 2** (Figure 1b,c). In Figure 2a, the reference melting peak of hTST without compounds is detailed. In this figure, 2 melt peaks were observed. Due to the low melting temperature of the first peak, this peak is considered to have been caused by protein instability caused by the presence of DMSO. The second peak, which has a melting point of 55°C, was used as the reference melting point. Figure 2b shows the melting curve of TST with **Hit 1**. In this experiment, the melting point of the protein was significantly increased to 76°C. Figure 2c shows a similar result for **Hit 2**, as the stability of the protein was determined in the presence of this compound was increased to 72°C. All other compounds identified from the preliminary screening tested either had no effect on the stability of the protein or decreased it and were discarded from further analysis. This provided a hit rate of ∼0.3% (2/623) from our initial screening. DSF methods are sensitive to the inherent fluorescence characteristics of the molecules present in the test screen. This sensitivity might lead to a broad range in the background of thermal profiles and false negatives. There is still a chance that screening components will interact with the reporting dye, even if the use of extrinsic dyes somewhat reduces this because their primary function is to dramatically enhance the unfolding signal (Gao et al., 2020).

2.2.1 | TST in vitro activity assays

Analysis of stereochemistry

A follow-up kinetic analysis of **Hit 1** and **Hit 2** (Figure 4a) demonstrated that, while **Hit 1** displayed a lower EC_{50}, **Hit 2** provided a significantly higher degree of activation (**Hit 1**∼ 150%; **Hit 2**∼ 250%)—albeit at slightly higher concentrations (EC_{50} **Hit 1**: 2.7 ± 6.1 μM; EC_{50} **Hit 2**: 17.0 ± 9.5 μM). We therefore continued our analysis focusing on the strongest activator identified (**Hit 2**). The best kinetic activity of hTST was determined to be after an incubation time of 8 min (Figure S1). As the initial compound from the screening (**Hit 2**) was present as a diastereomeric mixture (Figure 3), an assessment of the role of the stereocenters on activation was necessary. Resynthesis of **Hit 2** was than performed starting from both enantiomers of homocysteine, separately (Figure 3b). This allowed us to fix the first homo-cysteine
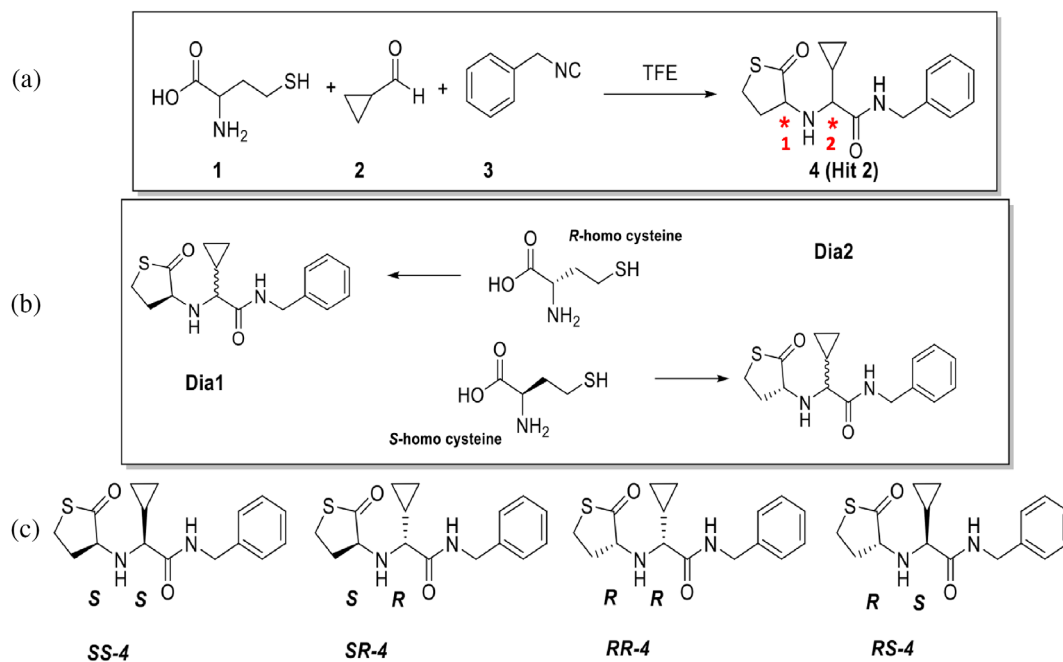
FIGURE 3 (a) **Hit 2** contains two stereo-centers (indicated by red asterisks) caused by the non-stereoselective reaction of homocysteine **1**, cyclopropanecarbaldehyde **2** and benzyl isocyanide **3** in 2,2,2-Trifluoroethanol (TFE) yielding the diastereomeric compound **4**. (b) To establish the role of these stereo-centers the synthesis was repeated using either S-homo-cysteine or R-homo-cysteine to yield compounds **Dia1** and **Dia2**, respectively. (c) While the identity of the first stereo center (*1: Figure 1a) can be thereby be determined, assignment of the second stereocenter (*2) cannot be made from the data from the chiral column alone.

stereo-center, but both products still were composed of a mixture of enantiomers with respect to the second stereo-center (Figure 3a). The products of these two syntheses were termed "**Dia 1**" and "**Dia 2**." When assays were performed to assess the impact on hTST activation, **Dia 1** showed an activation of ~200% with an EC_{50} of 32.8 ± 0.9 μM (Figure 4b) while, surprisingly, **Dia 2** showed a similar activation of ~250% with an EC_{50} of 28.5 ± 5.9 μM (Figure 4c). This implicates the first stereocenter on homocysteine as playing a role in the activation of hTST, with the mixture of the product of the reaction using S-homocysteine as starting material (**Dia 2**) showing marginally stronger activation.

However, it should be noted that the experiments detailed in Figure 4b,c do not provide a statistically significant difference in activation between the two separate diastereomeric mixtures. Additionally, neither **Dia 1** or **Dia 2** show a decrease in activation EC_{50} when compared with that seen in the unseparated mixture **Hit 2**, as may be expected if a single molecule responsible for activation had been enriched. Further diastereomer separation using chiral supercritical fluid chromatography (SFC; Figure S2) was performed on **Dia 1** and **Dia 2** to assess the activity of the separated four stereoisomers of **Hit 2** (Figure 3c). **Dia1** was separated into **Iso1** and **Iso 2**, while **Dia 2** was similarly separated into **Iso 3** and **Iso 4** (Figure S2B,C). Surprisingly, whereas the unseparated

mixture of **Dia1**, containing both **Iso1** and **Iso2**, showed activation of ~200%, the isolated isomers **Iso1** and **Iso2** both showed lower activation of hTST of ~120% (Figure 4d,e), with EC_{50}s of **Iso1** and **Iso2** of 29.8 ± 4.4 μM and 7.9 ± 3.4 μM, respectively. Similarly, where the unseparated mixture of **Iso 3** and **Iso 4** showed activation of ~250%, purified **Iso 3** showed activation of only ~150% (EC_{50} of 34.5 ± 4.8 μM; Figure 4f), and **Iso 4** showed an activation of approx. 125% (EC_{50} of 2.3 ± 4.2 μM; Figure 4g). The absolute assignment of the second stereo-center (*2, Figure 3a) still awaits confirmation and we cannot currently determine the relative importance of binding affinity or activation strength to the overall activation mechanism.

In summary, while the four individual isomers of this compound all show activation behavior, with a varying strength of interaction (EC_{50}) and degree of activation (~100%–150%) as expected for structurally distinct molecules, no significant improvement in the overall activation of hTST is seen when separating **Hit 2** into its component isomers. Conversely, a significant drop in overall activation is seen when isolating single isomers from those present in **Hit 2** (from ~250% to ~125%). Additionally, while **Iso 3** provided the highest degree of activation of the purified isomers, **Iso 4** showed the strongest binding EC_{50} to hTST. This data indicates that a mixture of isomers is required to achieve full activation of
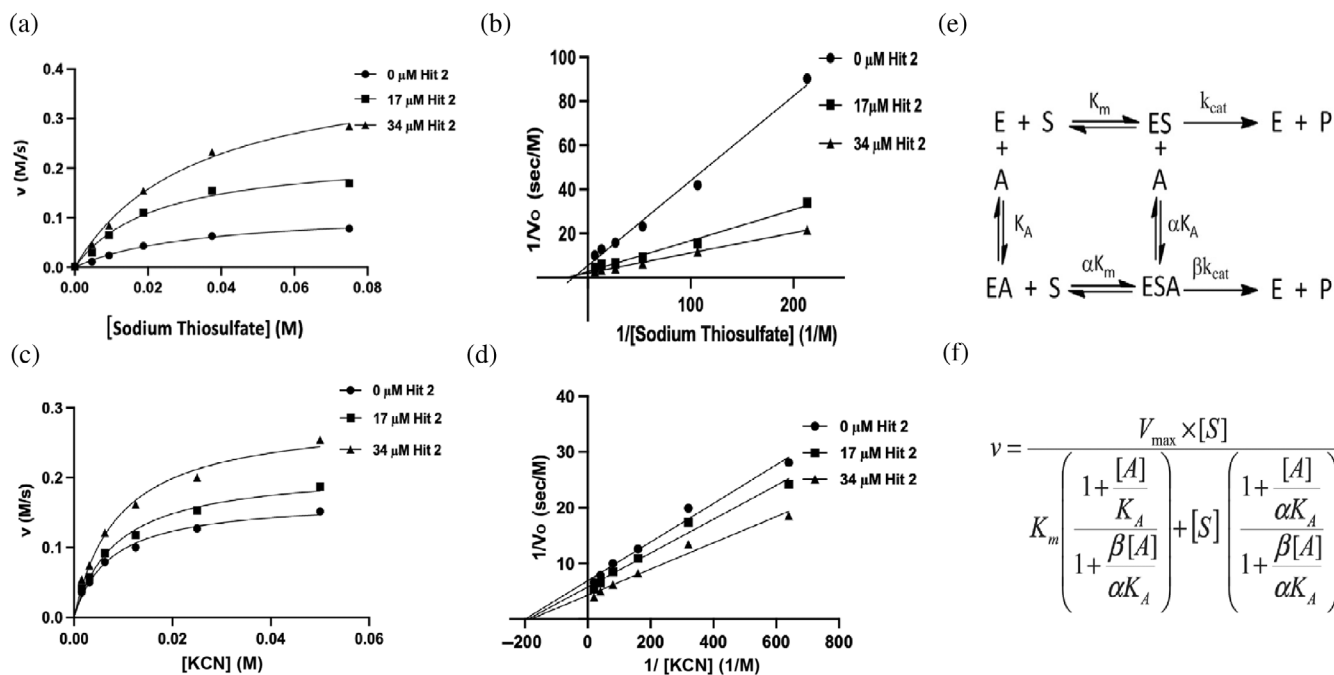
FIGURE 5 Steady-state kinetic characterization of the *h*TST versus the Sodium Thiosulfate concentration of activator **Hit 2**. (a) The Michaelis–Menten plots and (b) the Lineweaver–Burk plots show the relation of *h*TST activity versus the Sodium Thiosulfate concentration at three selected concentrations of **Hit 2** (·) 0 μM, (■) 17.1 μM, and (▲) 34 μM in the presence of 60 mM KCN substrate. Steady-state kinetic characterization of the *h*TST versus the KCN concentration of **Hit 2** activator. (c) The Michaelis–Menten plots, and (d) the Lineweaver–Burk plots show the relation of *h*TST activity versus the KCN concentration at three selected concentrations of **Hit 2** (·) 0 μM, (■) 17.1 μM, and (▲) 34 μM in the presence of 60 mM Sodium Thiosulfate substrate. (e) Scheme 1. Kinetic model for non-essential activation. (f) Equation 1 for the enzyme kinetics according to the model in Scheme 1. v is the reaction velocity, V_{max} is the maximal reaction velocity, [S] is the substrate concentration and K_m is the Michaelis–Menten constant, [A] is the activator concentration. α and β respectively, are the parameters to describe the change in the affinity of substrate binding and the change in the catalytic constant.

compound **Hit 2**. A potential explanation is that the activation mechanism results from an interaction of *h*TST with more than a single isomer of **Hit 2**, or that some form of assembly between distinct isomers of **Hit 2** is required for the activation mechanism. As none of the separated pools possessed improved activation properties when compared the initial mixture, we decided to proceed with further analysis using the mixture of isomers represented by the initial **Hit 2**.

Species selectivity of TST activation

Similar experiments using **Hit 2** against *ec*MST showed no activation of the protein, but an activation of ∼50% (EC50 12.9 ± 2.7 μM) when tested against *b*TST (Figure 4h). The active site of *h*TST is strongly conserved with that of *ec*MST and completely conserved for *b*TST. However, lower sequence conservation is present for the overall molecules, with the sequence identities to *h*TST for *ec*MST and *b*TST being 38% and 89%, respectively. This comparison strongly suggests that at least some of the enantiomers of **Hit 2** do not interact directly with the conserved active site amino acids. Instead, these molecules may interact allosterically with other surface amino acids that are conserved between *h*TST and *b*TST, but vary between *h*TST and *ec*MST. This potential for an allosteric mechanism of activation was further explored in both kinetics and molecular modeling experiments detailed below.

Microscale thermophoresis (MST) confirms a direct interaction between hit 2 and hTST

The binding affinity of **Hit 2** toward the protein *h*TST was analyzed using MST with the disassociation constant (K_d) determined to be 18.3 ± 0.8 μM, which indicate good binding of compound to *h*TST (Figure 4i). While the MST experiments cannot assign a unique binding constant for any of the isomers of **Hit 2**, the experiments described do further support a direct physical interaction between **Hit 2** and *h*TST, confirming the interpretation of the DSF results described above.

Enzyme kinetics support an allosteric activation mechanism

The capacity of *h*TST to detoxify cyanide via sulfur transfer from thiosulfate was assessed at different concentrations of **Hit 2**. From the dependence of the reaction rate

TABLE 1 Enzyme kinetic parameters for activation of hTST by Hit 2 versus sodium thiosulfate and KCN.

	Sodium thiosulfate			Potassium cyanide		
Compound Hit 2 (μM)	0	17.1	34.2	0	17.1	34.2
K_m (mM)	70.7 ± 7.8	51.1 ± 19.1	43.9 ± 3.6	5.02 ± 0.79	5.2 ± 0.98	5.5 ± 0.87
V_{max} (mM/s)	0.18 ± 0.01	0.37 ± 0.04	0.48 ± 0.02	0.14 ± 0.01	0.17 ± 0.01	0.23 ± 0.01
R^2	0.990	0.983	0.998	0.982	0.977	0.974
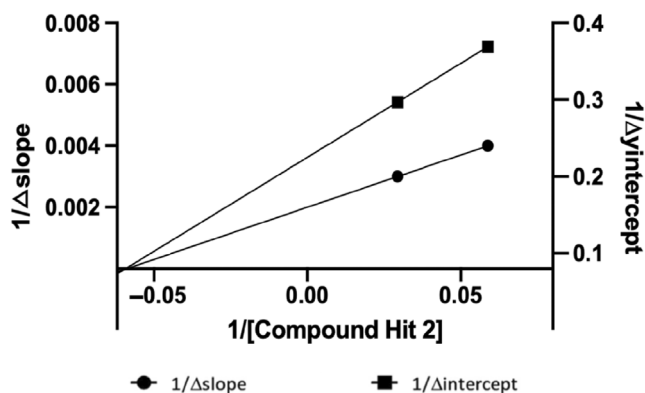
FIGURE 6 Re-plot of $1/\Delta$ slopes and $1/\Delta$ y-intercept versus concentration of **Hit 2**.

on substrate concentration, K_m values of $5.2 + 0.98$ mM for cyanide and 51.1 ± 19.1 M for thiosulfate were obtained at 17.0 μM concentration of **Hit 2**. The initial velocities of hTST were determined at various concentration of sodium thiosulfate, various concentrations of **Hit 2** (0, 17, and 34 μM), and a fixed concentration of potassium cyanide. The velocities were plotted in the Michaelis–Menten and the Lineweaver–Burk plot as shown in Figure 5a,b. The Michaelis–Menten analysis showed that **Hit 2** causes an increase in V_{max}, whereas the K_m is decreased (Table 1). Lineweaver–Burk analysis provided similar values. This indicates a non-essential mixed type activation and indicates that the activator can bind to both the free enzyme (E, Figure 5e) and to the substrate bound enzyme (ES, Figure 5e). In this model binding of sodium thiosulfate and the activator mutually influence each other. According to this model, the activation can be described by Equ.1 (Figure 5f; Leskovac, 1979).

The enzyme kinetics of **Hit 2** were further investigated through the Michaelis–Menten and the Lineweaver–Burk plots (Figure 5c,d) for various concentration of potassium cyanide. The initial velocities of hTST at different concentration of potassium cyanide and a fixed concentration of sodium thiosulfate and at several selected concentrations of **Hit 2** were measured. Activator **Hit 2** causes an increase in V_{max}, whereas the K_m values remain constant (Table 1). The values demonstrate non-competitive activation compared to potassium cyanide as a substrate in which binding of potassium cyanide is not influenced by the activator.

The enzyme kinetic parameters were derived as described in the material and methods using methods from Leskovac (1979). The activator dissociation constant (K_A), the change in the affinity of the substrate (α), and the change in the catalytic constant (β) were determined by re-plotting the slopes and the y-interceptions derived from the Lineweaver–Burk plot as a function of activator **Hit 2** in the same way as reported previously by Wisastra et al. (2013) (Figure 6). The kinetic analysis shows that α is 6.2, β is 5.5 and K_A is 15.2 μM.

A TST activator increases the mitochondrial respiration

To investigate whether a hTST activator could impact mitochondrial function and respiration, we performed experiments with isolated brain mouse mitochondria (Figure 7a). The oxygen consumption during basal respiration of the mitochondria was approximately 40 pmol/s/mL. Figure 7b shows the basal mitochondrial respiration (state 2) of the isolated mitochondria treated with the hTST activator, **Hit 2**, or vehicle using high-resolution respirometry. Interestingly, we found that TST activation by **Hit 2** (for a period of 25 min) in isolated mitochondria slightly increased the mitochondrial state 2 and state 3 considered as the ADP-stimulated mitochondrial respiration (state 3; Figure 7c). Likewise, high-resolution respirometry analysis indicated that **Hit 2** could promote an increase in maximum uncoupled respiration initiated by the addition of FCCP to the chambers where around 20% of state 3u increased compared with the vehicle compared to the control (Figure 7d). Further analysis showed that **Hit 2** did not affect other mitochondrial parameters, such as specific mitochondrial complex or non-mitochondrial respiration. However, in view of the results, the hTST activator is able to slightly enhance mitochondrial respiration compared to vehicle-treated brain purified mitochondria.

hTST protein modeling

The pBLAST search yielded five bTST sequences (1ORB, 1BOH, 1RHS, 1DP2, 1RHD) with 98%–99% identity to hTST (Kruithof et al., 2020). The bovine structures were chosen as protein modeling templates. With a Qualitative Model Energy Analysis (QMEAN) value of 0.71, the hTST model generated for the SWISS-MODEL server using the
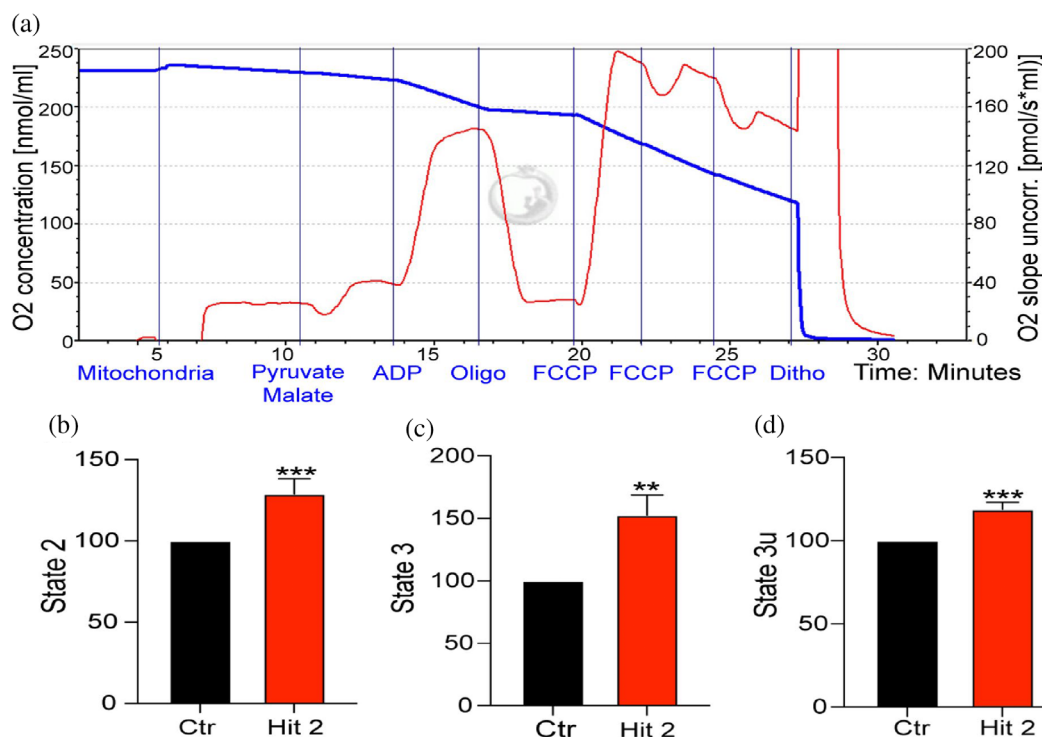
FIGURE 7 **Hit 2** increases the uncoupled respiration in isolated mitochondria. (a) Representative oxygen slope of isolated mitochondria. Definition of mitochondrial states (1, 2, 3, 3u) by addition of indicated substances in a representative measurement. (b) Quantification of state 2. (c) state 3 (ADP stimulated respiration). (d) state 3u (ETS, uncoupler FCCP titrations) of mitochondria pre-treated with vehicle (Ethanol, depicted as Ctr) or **Hit 2** (50 μM). Vehicle values are set at 100. Data are shown as mean ± SEM, $n = 3–4$ technical replicates; $n = 7$ biological replicates. p-values indicating statistically significant differences between the mean values are defined as follows: **$p < 0.01$, ***$p < 0.001$ drug versus control.

1DP2 crystal as a template represented the best model and was chosen for further experiments. The Ramachandran plot improved slightly after model refinement with Model-Refiner in the most favorable regions for protein residues in the α-helixs and β-sheets region (Figure S3A,B). Furthermore, after refinement, several faulty planarity groups or protein residues were improved (Figure S3C,D). As a result, the refined hTST model was used in docking and molecular dynamic experiments.

2.3 | Binding site identification

We used blind docking in conjunction with MD approach to identify the potential binding site of the isomers of **Hit 2**. We hypothesized that **Hit 2** would bind to an allosteric site in the enzyme based on the kinetic evidence that it was a non-substrate competitive activator of hTST and showed no activation of the ecMST homolog. As a result, we characterized the catalytic site in our hTST model based on previous reports (Gliubich et al., 1996; Kruithof et al., 2020). Our model accurately reproduced the substrate-specific CRKGVT motif required for interaction

with the negative charges on the substrate, as expected (Figure 8a) Furthermore, the CRKGVT contains the catalytic Cys248 required for hTST activity (Figure 8a; Gliubich et al., 1996; Guvench, 2015). A molecular docking over the hTST druggable pockets was performed using Ledock to assess the accessibility of **Hit 2** for the hTST surface and to find a potential binding mode. According to reports, this software is the most accurate option for reproducing and identifying potential crystallographic binding modes (Wang et al., 2016). Importantly, no specification of the stereo-chemistry was used, allowing the software to explore all 4 isomers. The main cluster of **Hit 2** binding modes was discovered in the catalytic domain (Figure 8b), which corresponds to its ability to bind organic compounds for catalytic conversion (Kruithof et al., 2020). Furthermore, a second activator second binding site was discovered on the opposite face of the hTST active site (Figure 8c). Interestingly, the pocket identification by MDpocket confirmed the presence and accessibility of the binding site identified by molecular docking (named site 1; Figure 8c). Our pocket identification experiments also revealed that the active site and site 1 are the most frequent and accessible during protein dynamics.
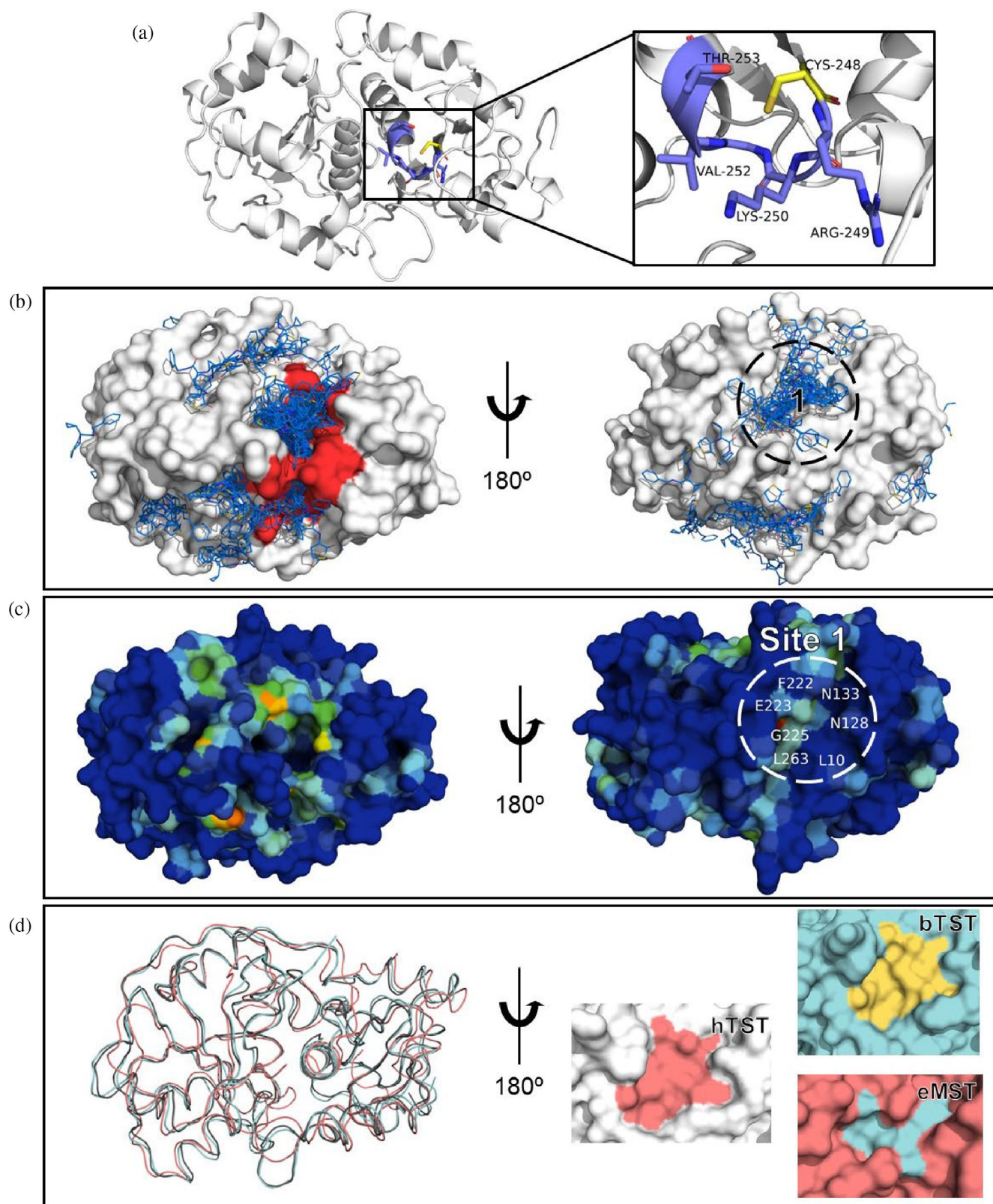
FIGURE 8 Identification of the binding site of Hit 2 binding site in *h*TST. (a) The *h*TST structure (gray) and the CRKGVT motive (blue and yellow sticks) with the catalytic Cys248 (yellow sticks). (b) Docking result of **Hit 2** in *h*TST, with the catalytic site highlighted in red surface. Site 1 is labeled and represented by a dashed circle. (c) MD and MDpocket analysis identified highly conserved pockets; site 1 is shown as a dashed circle. The frequency of appearance of the binding site is indicated by the blue-red color scale. (d) Structural alignment of modeled *h*TST(black), bovine TST (PDB 1RHD, cyan), and *E. coli* MST (PDB 1URH, red), the location of site 1 is represented as contrasted colored surface.

Finally, the structural comparison of *h*TST with available crystals of *b*TST (1RHD) and *ec*MST (1URH) showed a higher structural similarity between all the enzymes (Figure 8d). Moreover, differences in size and composition of the site 1 of all the enzymes might explain the changes of the activity of **Hit 2** in all the enzymes. For example, the differences between *h*TST, *b*TST, and *ec*MST might be due to the fact that the later exhibits a narrower allosteric site 1 making the fitting of **Hit 2** more restricted or perhaps impossible. As a result of our computational and structural analysis, we decided to investigate the binding of **Hit 2** in *h*TST in site 1 by MD.

2.4 | Molecular dynamics of *h*TST

The **Hit 2** liganded hTST model (Lig-*h*TST) simulation showed that **Hit 2** remained bound stably in site 1 for at least 100 ns (Figure 9a). Calculation of the binding free energy (Figure 9b,c) of **Hit 2** showed that van der Waals' energetic component contributes most to the total binding energy. Moreover, the energetic profile indicated low fluctuations on the *h*TST. Suggesting a stable binding mode during the first 100 ns of the simulation. The binding of **Hit 2** to *h*TST is supported by energetically favorable interactions with residues Leu6, Ala9, Leu10, and Tyr262, according to per-residue energetic decomposition (Figure 9d,f,g). Furthermore, molecular interactions revealed that Leu6, Ala9, and Leu10 are involved in frequent H-bonds, and that Leu6 and Tyr262 are involved in hydrophobic interactions (Figure 9e,g). Finally, the formation of water bridges between **Hit 2** and the Arg8 is a very common interaction (Figure 9e,g). To better understand the role of **Hit 2** in *h*TST activation, we compared the MD trajectories of the Lig-*h*TST, unliganded *h*TST (apo-*h*TST), and an inactive C248A mutant (Ala-*h*TST) systems. The pairwise root mean square deviation RMSD analysis revealed no significant differences in the protein's overall flexibility (Figure S4A). This suggests that the binding of **Hit 2** or the presence of the inactivating C248A mutation has no effect on protein conformation when compared to functional *h*TST (apo-*h*TST). Nonetheless, the root mean square fluctuation (RMSF) analysis revealed a slight increase in the *h*TST fluctuations in the Lig-*h*TST and Ala-*h*TST systems (Figure S4B). Surprisingly, such fluctuation increases occur in the loops that comprise the catalytic site (Figure S4C). In accordance with this discovery, we observed an increase in the pocket density of the active site in the Lig-*h*TST and Ala-*h*TST systems. These findings suggested that the catalytic site's properties changed as a result of **Hit 2** or the inactivating mutation C248A.

A physicochemical characterization of the *h*TST catalytic site was performed in order to analyze potential changes in the active site. Surprisingly, the most significant changes in *h*TST with **Hit 2** occur during the first 100 ns of simulation, when the compound is stably bound to the enzyme (Figure S4E–J). The binding of **Hit 2** increases the pocket volume of the active site of *h*TST while keeping the volume of the apo-*h*TST and Ala-*h*TST forms constant (Figure S4A). Similarly, an increase was observed for the Solvent Accessible Surface Area (SASA) and both polar and apolar components. These findings might imply that the *h*TST active site could be more easily accessed by its substrates (Figure S4F–H). Moreover, the proportion of polar atoms increased in the Lig-*h*TST and Ala-*h*TST when compared to the apo-*h*TST (Figure S4I). Furthermore, during the majority of the simulation, an increase in the charge score, defined as the mean charge for all amino acids identified in the pocket, was observed (Figure S4J). This is especially significant given that it has been reported that the activity of *b*TST is dependent on the stabilization of the negative part of the substrate by the positive charges of Arg186 and Lys249, which have corresponding residues in *h*TST as Arg187 and Lys150 (Gliubich et al., 1996; Kruithof et al., 2020). As a result, an increase in the positive charge in the active site of *h*TST could have a direct effect on the enzyme's activity.

In summary, the Ala-*h*TST had a similar volume and SASA to the apo-*h*TST, but a higher number of polar atoms and a higher overall charge score. An increase in volume, SASA, polar/apolar SASA, the proportion of polar atoms, and a slight increase in positive charge could explain why **Hit 2** could activate *h*TST due to a facilitation of substrate binding to the catalytic site via a more accessible volume and surface, as well as an improvement in the stabilization of the negative charges on the substrate by the positively charged residues in the catalytic site.

3 | DISCUSSION

TST was originally discovered as a cyanide detoxification enzyme, but several other functions for the enzyme have since been suggested (Gnaiger, 2014; Morton et al., 2016). The ability of the enzyme to efficiently work with highly reduced sulfur indicates several possible functions. Two of the major mitochondrial antioxidant systems (glutathione and thioredoxin) are thiol-dependent, and TST may function as one of their sources for reducing equivalents (Morton et al., 2016). This function of TST would allow the mitochondria to scavenge reactive oxygen species at a
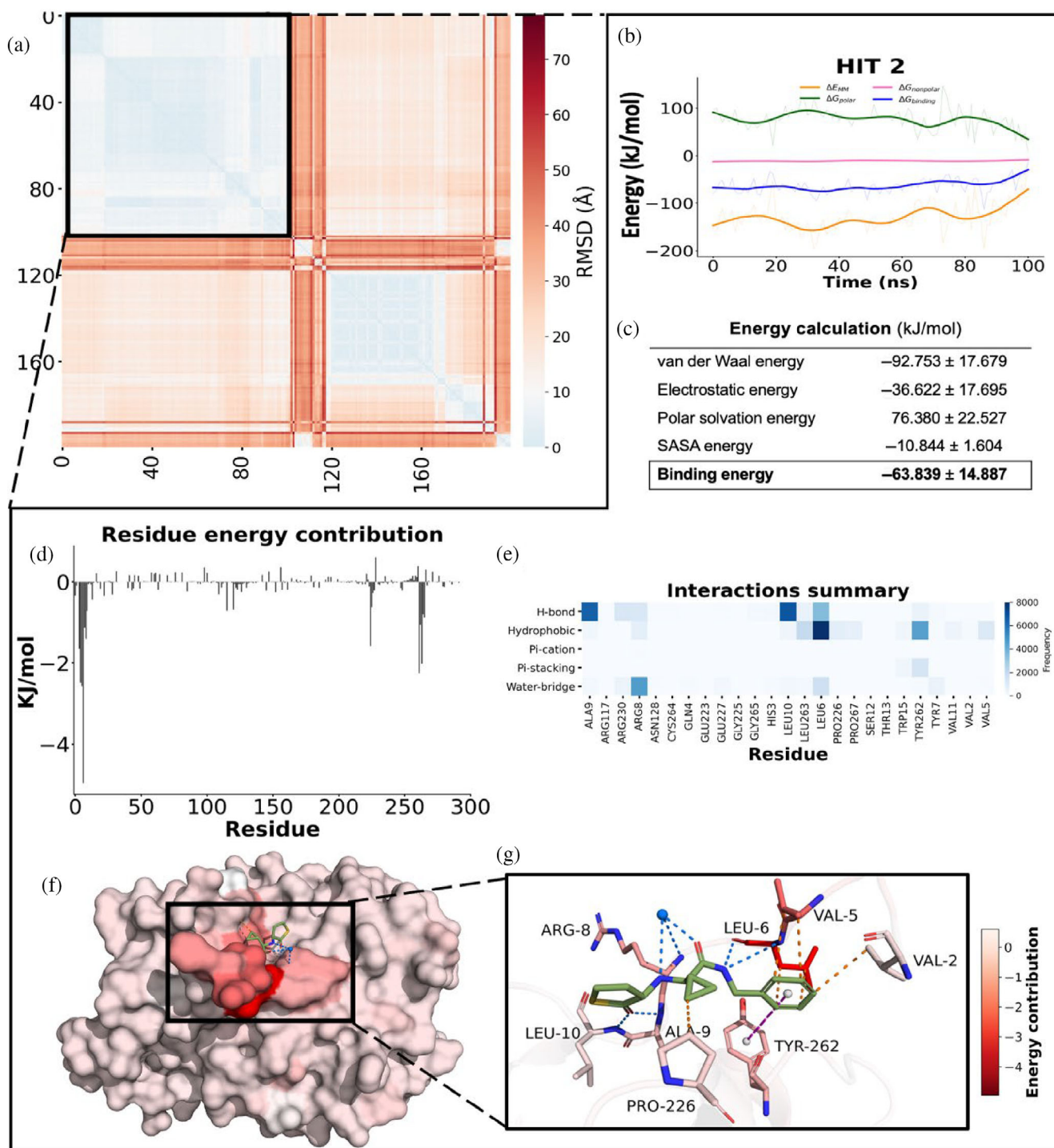
FIGURE 9 Binding energy and molecular interactions of compoun1 with *h*TST. Pairwise RMSD of **Hit 2** binding poses over the course of 200 ns of simulation. The black box denotes **Hit 2**'s stable binding to site 1 (100 ns). (b) **Hit 2**'s energetic decomposition based on MM/PBSA calculations. (c) Table of the contribution of energy components computed from MM/PBSA and calculated binding energy of **Hit 2** to *h*TST. (d) Energy contribution per residue. Val2, Leu6, Val5, Arg8, Ala9, Pro226, and Tyr262 have the most negative values. (e) The types and frequency of interactions that support stable **Hit 2** with *h*TST interactions. (f) The per-residue energy decomposition is mapped in 3D by the *h*TST structure. (g) The molecular interactions and potential binding mode of one isomer of **Hit 2**: ((2R)-N-benzyl-2-cyclopropyl-2-{[(3S)-2-oxothiolan-3-yl]amino}acetamide), are depicted in a representative frame from Lig-*h*TST MD (green sticks). *h*TST carbon residues are colored according to the per-residue decomposition scale, with water molecules represented by blue spheres, hydrogen bonds represented by blue dashes, π-stacking represented by magenta dashes, and hydrophobic interaction represented by orange dashes.

higher rate, thereby preventing mitochondrial damage. Additionally, sulfur can be used to complex both iron and selenium atoms, and both complexes are required for the function of many other proteins (Selles et al., 2019; Xu & Zhang, 2011) Iron–sulfur complexes are integral to the function of complex I-IV (CI-CIV) in the electron transport chain, as they function as electron carriers (Selles et al., 2019). Selenium-sulfur complexes are integral to the function of selenocysteine proteins, which function as another important class of ROS-scavengers (Xu & Zhang, 2011). It should be mentioned that although while these functions of complex I-IV (CI-CIV) are compelling, they have not yet been thoroughly researched.

In this report, we describe the identification of a novel activator of TST that is selective between the TST of different species. ($\sim$250% activation in hTST, $\sim$50% in bTST, and 0% in ecMST). Separation of **Hit 2** into its respective enantiomers did not identify a single isomer that was as potent as the mixture represented by **Hit 2**, suggesting that two or more **Hit 2** molecules of different stereo chemistry are needed for maximal activation. This result has been confirmed in multiple resyntheses of **Hit 2**. Kinetic analyses suggest at least one binding site for **Hit 2** that is conserved between hTST and bTST, but distinct in ecMST and potentially distal to the TST catalytic site. This is supported by the modeling data, that identifies a potential pocket for **Hit 2** binding over 23.4 Å from the hTST active site.

A steady-state enzyme kinetic analysis of hTST in the presence of the activator **Hit 2** was performed in order to determine the activation mechanism. The kinetic characterization of hTST activity versus various concentrations of the **Hit 2** at fixed concentration of potassium cyanide and sodium thiosulfate shows a concentration dependent activation. The results from the non-linear curve fitting were in line with the results from Lineweaver–Burk plot and demonstrate non-essential mixed type activation. This indicates that the activator can bind to the free enzyme and also to the substrate bound enzyme. In this model binding of the substrate and **Hit 2** mutually influence each other.

The dissociation constant, $K_A = 15.2\,\mu M$, in micromolar range shows a reasonably high potency of **Hit 2** as an activator of hTST. The K_A value (15.2 μM) is similar to the K_d (18.3 μM), which also indicates the binding of the compound to hTST. The α value, which indicates the change in substrate binding, gives about 150% enhancement of substrate binding to the activator bound enzyme compared to the free enzyme. The catalytic constant for substrate conversion reaction was enhanced by 5.5-fold in the presence of the activator compared to the normal reaction conditions. From these parameters we can conclude that **Hit 2** gives a non-essential mixed-type activation of hTST and binds with high affinity ($\alpha K_A = 93.3\,\mu M$) to the substrate bound enzyme and enhances the conversion of the cyanide to thiocyanate.

The Oroboros method uses isolated mitochondria from mouse tissue and can give a strong indication of the effects of the compound in vivo. It can predict the oxidative phosphorylation which is a central energy-conserving mechanism, coupling mitochondrial electron transfer to ATP synthesis and providing the energy required for the maintenance of cellular functions and cell survival. Assessment of mitochondrial respiration represents a functional evaluation of mitochondrial homeostatic state (Gnaiger, 2014). To assess the potential of **Hit 2** in a cellular context we performed assays on isolated mitochondria. The isolated mitochondria showed the ability to metabolize the provided pyruvate and malate at a slowly declining rate. Also, it was able to complete its metabolic cycle in the presence of ADP and were able to produce ATP from the metabolites provided earlier, consuming oxygen in the process. The oxygen concentration was measured, and the rate at which the oxygen concentration declines was projected as the measure for respiratory speed. The respiratory speed of the mitochondria increased when an activating substance for hTST was given, but not beyond its normal limit. The increase in the respiration found in the mitochondria is unlikely to be the result of cyanide detoxification or ROS-scavenging. The concentration of cyanide in the mitochondria is very low, and ROS-scavenging might increase the lifetime of the mitochondria. Low cyanide concentrations induced mitochondrial electron transport stimulation and increased intracellular adenosine triphosphate (ATP), which induced between TST and proteins in the electron transport chain. Increased availability of iron–sulfur complexes in the mitochondria might lead to an increase in constituted CI-CIV, which in turn could speed up oxygen consumption (Xu & Zhang, 2011).

In summary, we describe the first small molecule activator (**Hit 2**) of this enzyme, with a potency in the low micromolar range that provides a clear and concentration dependent activity enhancement. Direct physical interaction is supported by both DSF and MST data. Enzyme kinetic analysis revealed an activator dissociation binding constant K_A of 15.2 μM and activity enhancement of the K_{cat} by a beta value of 5.5, which is in line with other observations in this report. Analysis of the separated isomers suggest that two or more isomers of **Hit 2** are needed simultaneously to reach full activation. Oroboros analysis showed that this compound increased Complex I-linked respiration rate, induced by ADP (state 3) by approximately 50% above the control and increased the maximum uncoupled respiration induced by FCCP by

20% relativity to the control. The vitro and ex vivo studies of **Hit 2** presented here show that this compound influences the activity of _h_TST which make this compound an interesting molecule, the study of which would help to develop drugs for diabetic and other diseases. Further development of this compound could help to enhance its activity and extra cellular studies are required to understand the activity of this compound in vivo. Overall, this novel compound is a promising lead to develop therapeutics to reduce the risk of diabetic and other diseases. Clarification of the binding mode(s) of the individual isomers present in **Hit 2** require structural analysis, which is currently underway.

4 | MATERIALS AND METHODS

4.1 | Expression and purification of hTST, ecMST, and bTST

A synthetic gene for _hTST, ec_MST, and _b_TST codon-optimized for _E. coli_ (Eurofins) were cloned into the pETM11 vector (Dümmler et al., 2005). Successful cloning was confirmed by Sanger sequencing. The resulting product was used to transform R2P competent cells (Novagen). The expression plasmid and a glycerol stock were prepared and frozen at −80°C for further use. This stock was used to inoculate 20 mL LB media supplemented with 100 mg/L kanamycin and 2 mM magnesium chloride. After overnight incubation at 37°C this mini-culture was used to inoculate 2 L of TB media supplemented with 100 mg/L kanamycin and 2 mM magnesium chloride, which was induced with 0.4 mM Isopropyl β-D-1-thiogalactopyranoside (IPTG) at OD600 ≈ 1.2. The cultures were grown overnight at 18°C. The fully-grown cultures were spun at 10,000 g for 30 min. The pellets were resuspended in Lysis buffer (100 mM Tris–HCl, 300 mM NaCl, 20 mM imidazole, 5% v/v Glycerol, and 5 mM BME at pH 8.0), which were incubated with DNAse1 and Lysozyme for 30 min. Afterward, the resuspended pellets were sonicated on ice. The lysate was then spun at 41,000 g for 45 min. The supernatant was run on His-tag purification, and the elution was tested on SDS-gel electrophoresis. The elution was purified with size-exclusion chromatography and the purity of the protein was tested on SDS-gel electrophoresis.

4.2 | Screening of the small molecule library

In order to find potential activators for the _h_TST enzyme, an assay utilizing the conversion of cyanide to thiocyanate by _h_TST was established. In the initial screening assay, 623 unique chemical entities synthesized in-house were screened (Dömling, 2006; Dömling et al., 2012). In this screening, every compound tested was assigned with 2 wells on a 96 wells plate. Of these wells, one was filled with all the chemical components needed for a complete enzymatic conversion from cyanide to thiocyanate (Libiad et al., 2018; Sörbo et al., 1953). This well contained 53 μL of protein buffer containing 300 mM (2-[4-(2-hydroxyethyl)piperazin-1-yl]ethanesulfonic acid) (HEPES), 150 mM NaCl, 77 mM sodium thiosulfate and 28 ng/mL TST. A total of 1 μL of compound solution (1 mM final concentration from stock solutions of 1 M compound in 100% DMSO) was added to the reaction followed by the addition of 10 μL of 500 mM potassium cyanide (KCN). The other well was used as a control which lacked KCN but contained the same concentrations of all other components. Three wells per plate were used for references which contained the same reagents with the exception of the compound. The reaction was allowed to take place for 20 min after which it was stopped by adding 7 μL formaldehyde. The amount of thiocyanate in each well could then be determined by adding 30 μL 300 mM ferric nitrate in a 10% nitric acid solution. After adding ferric nitrate, the absorbance of all wells was measured at 460 nm.

Absorption from wells with compound was compared to those with DMSO and the blanks were used as correction for innate absorption of the compounds and the assay materials in general. After initial screening, the most promising compounds were re-screened in triplicate using a setup in which 8 wells were assigned per test-compound. Out of these 8 wells, 3 contained all components for the complete reaction in the concentrations described above, another 3 were used as reference and contained DMSO instead of compound. The final 2 wells contained blanks which lacked KCN and contained either DMSO or the compound. After the second screening was completed, the assay was run a third time using blanks that did not contain _h_TST protein.

4.3 | Substrate kinetics hTST, ecMST, and bTST in vitro assays

In order to determine the substrate kinetics of _h_TST, colorimetric assays were performed at 23°C as described previously with minor modifications (Libiad et al., 2018; Sörbo et al., 1953). The enzyme activity was measured in the absence or presence of activator **Hit 2** at fixed concentrations (0, 17, and 34 μM). The reaction velocities (v), which represent the concentration changes over time, were plotted against the substrate concentrations in

Michaelis–Menten plots to determine the K_m and V_{max} in the presence of the activator.

The substrate kinetics for thiosulfate were measured by incubating 20 nM hTST with 60 mM potassium cyanide (KCN) and different concentrations of sodium thiosulfate (0–100 mM) for 8 min, in 300 mM HEPES pH 7.4, 150 mM NaCl. The reaction was quenched using 10 μL of 15% (w/v) formaldehyde, followed by the addition of a ferric nitrate solution (165 mM ferric nitrate nonahydrate, 13.3% (v/v) nitric acid) (100 μL) to form a ferric thiocyanate complex. Thiocyanate concentrations were determined from the absorbance at 460 nm. The substrate kinetics for potassium cyanide (KCN) were measured in the same way; however, the sodium thiosulfate concentration was fixed at 60 mM, and different concentrations of potassium cyanide (KCN) were added (0–100 mM).

The slopes and y-intercepts from the Lineweaver–Burk plot of hTST activation was obtained and then re-plotted as 1/Δslope or 1/Δy intercept versus 1/[activator]. The values of α, β, and K_A were calculated from these plots as described by Leskovac (Leskovac, 1979) for non-essential activation.

The y intercept in the re-plot of 1/Δy intercept versus 1/[activator] corresponds to β($V_{max}/(β-1)$), while in the re-plot of 1/Δslope versus 1/[activator], the y intercept corresponds to β. V_{max}/K_m (β−α). The x intersection point of two lines from the plot of 1/Δy intercept and 1/Δslope is −β/αK_A, which can be used to calculate the K_A value.

In order to measure the catalytic reactivity of the protein in the presence of compounds, the same assay was used to screen different concentrations of **Hit 2** (0.244–500 μM). The same protocol was used to check the catalytic reactivity of the proteins ecMST and bTST in the presence of the identified activator **Hit 2**.

4.4 | Differential scanning fluorimetry (DSF)

DSF was run as an initial assay in order to give an indication of binding between the selected compounds and the enzyme TST. This assay allows for changes in the stability of proteins to be detected by determining the temperature at which they unfold. An increase in protein stability in the presence of a compound indicates that binding has taken place. Data collection is made possible by using the fluorescent dye SYPRO orange. This dye is able to bind to hydrophobic parts of proteins that only become available for binding upon unfolding of the protein. The solution used for the screening consisted of 5× SYPRO orange dye, 500 μL of 2 mg/mL protein and 4 mL size exclusion buffer. Of this mixture 45 μL was pipetted in each well to which 5 μL of compound (100 mM in 100% DMSO) or DMSO was added. During the experiment, the temperature of the samples was increased by 0.5°C per minute starting at 20°C and ending at 95°C. Unfolding was followed by measuring the fluorescence of the samples.

4.5 | Microscale thermophoresis (MST)

The binding affinity of compounds toward TST protein were analyzed using MST. First, affinity experiment was performed to determine the affinity and labeling efficiency of dye to TST. Next, TST protein and compounds at gradient concentration were prepared following Monolith His-Tag Labeling Kit RED-tris-NTA protocol with PBS-T buffer (PBS pH 7.4, 0.05% Tween 20). Finally, binding affinities were calculated according to MST dose–response curve using 40% excitation power, high MST power, and red excitation type at 25°C.

4.6 | Resynthesis of Hit 2

General procedure, homocysteine (270 mg, 2 mmol) are solubilized in trifluorethanol (TFE) (10 mL) and cooled under nitrogen to −20°C. A solution of isocyanide (2 mmol) and aldehyde (2 mmol) in TFE (5 mL) are added dropwise. The reaction mixture is stirred for 1 h in the cold and allowed to warm to room temperature and stirred overnight. The solvent is evaporated and the crude product is purified by column chromatography on silica gel with heptane/EtOAc elution gradient from 3/1 to 1/2 (Figure 3).

4.7 | Separation of the stereoisomers

To further characterize the most active isomer of **Hit 2**, we separated the stereoisomers using semi-preparative supercritical fluid chromatography (SFC) on a Chiralpak IG chiral column, 10.0 × 250 mm^2 mobile phase CO2/MeOH 25% isocratic (Figure S2).

4.8 | Animals

C57BL/6 J mice from the central animal laboratory at University of Groningen were housed and handled in accordance to Dutch standards and guidelines. All experiments were approved by the University of Groningen Committee for Animal Experimentation.

4.9 | Mitochondrial isolation

The cortexes from brain tissue of C57BL/6 J mice were collected and harvested in 1.2 mL isolation buffer (300 mM sucrose, 5 mM TES, and 200 μM EGTA adjusted to pH 7.2). Crude mitochondria were isolated from the brain tissues utilizing semi-automated pump-controlled cell rupture system using syringes (SGE, Trajan© Scientific, Australia) linked to a cell homogenizer (Isobiotech, EMBL Heidelberg, Germany) and a pump (0.71 mL/min) (ProSense, Oosterhout, NL, #NE1000). Following passing the lysate through the homogenizer, the lysate was centrifuged and the crude mitochondria were re-suspended in isolation buffer containing 70 mM sucrose, 210 mM mannitol, 5 mM HEPES, and 1 mM EGTA adjusted to pH 7.2. The entire procedure was performed on ice (Krabbendam et al., 2020).

4.10 | High-resolution respirometry assay

The amount of protein used to determine mitochondrial respiration was 250 μg, as determined by the Pierce™BCA Protein Assay Kit (Pierce™BCA Protein Assay Kit, Thermo Scientific, Rockford, USA, #23225). The mitochondrial respiratory parameters were assessed by using the high-resolution respirometry oxygraph O2K (Oroboros Systems, Innsbruck, Austria). Isolated mitochondria prepared were treated with 50 μM of **Hit 2** or ethanol for 25 min and immediately loaded into the O2K instrument for respiration measurements. Mitochondrial states were monitored as followings: state 1 in 1 mL MiR05 buffer containing EGTA 0.5 mM, $MgCl_2$ 3 mM, lactobionic acid 60 mM, taurine 20 mM, KH_2 PO_4 10 mM, HEPES 20 mM, D-Sucrose 110 mM, BSA, essential fatty acid-free1g L^{-1}, at 7.4 pH, under continuous stirring at 750 rpm (Gnaiger et al., 2000). For the analysis, we used oxygen polarography, DatLab software (Oroboros Systems, Innsbruck, Austria) which was implemented to record real-time oxygen flux per tissue mass (pmol O2. $s^{-1}*mg^{-1}$) at 37°C. The Oroboros method was performed according to a previously established protocol (Krabbendam et al., 2020; Rosenbusch et al., 2021). Mitochondrial non-phosphorylating respiration, assessed as state 2 was monitored by addition of complex-I linked substrates, such as pyruvate (5 mM, Sigma-Aldrich Chemie GmbH, Steinheim, Germany #P-2256), and malate (2 mM, Sigma-Aldrich Chemie GmbH, Steinheim, Germany, #374318). Afterward, the oxidative-phosphorylation capacity, assessed as OXPHOS, State 3 of complex-I linked activity was measured following the addition of saturating concentration of ADP (0.8 mM, Sigma-Aldrich Chemie GmbH, Steinheim, Germany,

#A5285). Subsequently, to block Fo of the ATP-synthase, thereby inhibiting proton passage, we added oligomycin (0.1 μM ml^{-1}, Sigma-Aldrich Chemie GmbH, Steinheim, Germany, #O4876) was used. Next, maximal respiration, assessed as State 3 u was monitored by incremental steps of 1 μM of the FCCP, Sigma-Aldrich Chemie GmbH, Steinheim, Germany, #C2920. Sodium dithionite (DTT, Sigma-Aldrich Chemie GmbH, Steinheim, Germany, #15,795-3) was used at the end of measurements to react with all the oxygen present in the chamber. The oxygen concentration as well as the initial derivate of the oxygen concentration which is a derivative of the oxygen consumption is provided as the O_2 slope (pmol * (mL s^{-1}) of raw isolated mitochondria. The measurements were recorded in intervals of 2 s using instrumental background correction after calibration of the polarographic oxygen sensors. The data were analyzed using Datlab software. Signal after the quenching with sodium dithionite was assumed to be a measurement artifact, and subtracted from all other data points. Data points for the treatments versus control represent the change in oxygen consumption due to the treatment.

4.11 | *h*TST protein modeling

Due to the lack of crystal structures of the human thiosulfate sulfurtransferase (*h*TST) and a high homology between hTST and bTST (>96%), the protein structure was modeled using the primary sequence from UniProt (Q16762). A pBLAST was conducted using the *h*TST sequence as reference in the Protein Data Bank (PDB) database. The *h*TST model was created using the SWISS-MODEL server (https://swissmodel.expasy.org/; Biasini et al., 2014). In order to fix potential distance and angle errors in the residues of the model, a model refinement was carried out using ModelRefiner (Xu & Zhang, 2011). After the refinement, the model was analyzed by Procheck (Laskowski et al., 1993) to determine the final quality of the generated *h*TST model for future experiments.

4.12 | Binding site identification

The previously generated *h*TST refined model was used for blind docking using LeDock (Liu & Xu, 2019) and Fpocket (Le Guilloux et al., 2009) to detect the binding site of **Hit 2** using the blind docking protocol of Jupyter Dock (Moreno, 2021). The refined *h*TST model was used as a receptor in the docking experiments, and it was prepared by removing co-crystallized waters, solvent molecules, and adding charges and hydrogens with LePro (Liu & Xu, 2019). **Hit 2** was prepared by adding explicit

hydrogens and tautomeric states at pH 7.4. and generating 3D coordinates with MarvinSketch (http://www.chemaxon.com). The molecular docking was performed into all druggable pockets *hTST* identified by Fpocket requesting 50 poses per pocket. Besides, the binding site of **Hit 2** was also investigated by detecting highly conserved pockets during the 200 ns molecular dynamics simulation (MD) of *hTST* using MDpocket tool from Fpocket (Le Guilloux et al., 2009). The clustering of the binding poses and MDpocket analysis were employed to evaluate the binding of Hit 2 to the *hTST* surface.

4.13 | Molecular dynamics

Gromacs 5.0.4 (Abraham et al., 2015) was used to run the MD simulations. 3 MD simulations were performed in triplicate and no considerable differences were observed among the different runs Figure S5. Three systems were created, the apo-*hTST*, the Hit 2-*hTST* complex (lig-*hTST*), and a C248A mutation *hTST* (ala-*hTST*) as the inactivate state of *hTST*. The CGenFF and CHARMM36 force fields were used to parameterize the **Hit 2** and *hTST* proteins, respectively, using the CHARMM-GUI (http://www.charmm-gui.org; Allouche & rahman., 2012). Using the CHARMM-multicomponent GUI's assembler, the systems were built by adding TIP3P water molecules, neutralizing ions, and establishing periodic boundary conditions (PBC). The systems were minimized and then equilibrated under an NVT assembly prior to production. An NPT assembly was performed at 310.15 K for 200 ns during the production phase, saving velocities, energy, and positions every 10 ps. MDAnalysis (Gowers et al., 2016)was used to perform root mean square deviation (RMSD) and root mean square fluctuation (RMSF) analysis, and the molecular interactions of the Lig-*hTST* complex were performed using a tailor-made python script (https://github.com/AngelRuizMoreno/Scripts Notebooks/blob/master/Scripts/plipMDV3.1.py) with PLIP as engine (Salentin et al., 2015). The MDpocket module of Fpocket was used to perform the physicochemical characterization in the catalytic site in the systems (Le Guilloux et al., 2009). The first 100 ns of Lig-*hTST* trajectory was employed for free energy calculation using the molecular mechanics energies combined with the Poisson–Boltzmann surface area continuum solvation (MM/PBSA; Genheden & Ryde, 2015) by gmmpbsa v1.6 package (Kumari et al., 2014). To calculate the average binding energy, the potential energy in vacuum, polar solvation energy, and non-polar solvation energy were computed. Per-residue energetic decomposing and maps were created to map the contribution of each residue to the binding energy.

4.14 | Statistical analysis

The average of the triplicate value and their associated standard deviations were calculated. All calculations were performed with Excel 2010 and Graph Pad version 9.3. Oxygen flux were recorded in real-time using the DatLab software and the data were analyzed with DatLab5 (version 5.1.1.91). Data were presented as mean ± SEM.

AUTHOR CONTRIBUTIONS
Zayana M. Al-Dahmani designed, performed, analyzed experiments, and wrote the manuscript. Mojgan Hadian, Fernando A. Batista, Afsaneh Sadremomtaz, Mette Spoor, Ran Zhang, performed experiments. Afsaneh Sadremomtaz provided animal models. Angel J. Ruiz-Moreno, Afsaneh Sadremomtaz, providing protein modeling. Frank J. Dekker, Matthew R. Groves, Harry van Goor, Amalia M. Dolga, analyzed experiments, data interpretation, and drafted and revised the manuscript. All authors read and approved the final manuscript.

ORCID
Zeyana M. Al-Dahmani https://orcid.org/0000-0001-8860-4404

REFERENCES
Abraham MJ, Murtola T, Schulz R, Páll S, Smith JC, Hess B, et al. Gromacs: high performance molecular simulations through multi-level parallelism from laptops to supercomputers. SoftwareX. 2015;1-2:19–25. https://doi.org/10.1016/j.softx.2015.06.001

al-Dahmani ZM, Li X, Wiggenhauser LM, Ott H, Kruithof PD, Lunev S, et al. Thiosulfate sulfurtransferase prevents hyperglycemic damage to the zebrafish pronephros in an experimental model for diabetes. Sci Rep. 2022;12(1):12077. https://doi.org/10.1038/s41598-022-16320-1

Allouche AR. Software news and updates Gabedit—a graphical user Interface for computational chemistry softwares. J Comput Chem. 2012;32:174–82. https://doi.org/10.1002/jcc

Aminlari M, Malekhusseini A, Akrami F, Ebrahimnejad H. Cyanide-metabolizing enzyme rhodanese in human tissues: comparison with domestic animals. Comp Clin Path. 2007;16(1):47–51. https://doi.org/10.1007/s00580-006-0647-x

Biasini M, Bienert S, Waterhouse A, Arnold K, Studer G, Schmidt T, et al. SWISS-MODEL: modelling protein tertiary and quaternary structure using evolutionary information. Nucleic Acids Res. 2014;42:252–8. https://doi.org/10.1093/nar/gku340

Billaut-Laden I, Allorge D, Crunelle-Thibaut A, Rat E, Cauffiez C, Chevalier D, et al. Evidence for a functional genetic polymorphism of the human thiosulfate sulfurtransferase (Rhodanese), a cyanide and H2S detoxification enzyme. Toxicology. 2006;225(1):1–11. https://doi.org/10.1016/j.tox.2006.04.054

Bonadonna RC, Leif G, Kraemer N, Ferrannini E, Del PS, DeFronzo RA. Obesity and insulin resistance in humans: a dose-response study. Metabolism. 1990;39(5):452–9. https://doi.org/10.1016/0026-0495(90)90002-T

Dömling A. Recent developments in isocyanide based multicomponent reactions in applied chemistry. Chem Rev. 2006;106(1):17–89. https://doi.org/10.1021/cr0505728

Dömling A, Wang W, Wang K. Chemistry and biology of multicomponent reactions. Chem Rev. 2012;112(6):3083–135. https://doi.org/10.1021/cr100233r

Dümmler A, Lawrence AM, de Marco A. Simplified screening for the detection of soluble fusion constructs expressed in E. coli using a modular set of vectors. Microb Cell Fact. 2005;4:1–10. https://doi.org/10.1186/1475-2859-4-34

Gao K, Oerlemans R, Groves MR. Theory and applications of differential scanning fluorimetry in early-stage drug discovery. Biophys Rev. 2020;12(1):85–104. https://doi.org/10.1007/s12551-020-00619-2

Genheden S, Ryde U. The MM/PBSA and MM/GBSA methods to estimate ligand-binding affinities. Expert Opin Drug Discov. 2015;10(5):449–61. https://doi.org/10.1517/17460441.2015.1032936

Gliubich F, Gazerro M, Zanotti G, Delbono S, Bombieri G, Berni R. Active site structural features for chemically modified forms of rhodanese. J Biol Chem. 1996;271(35):21054–61. https://doi.org/10.1074/jbc.271.35.21054

Gnaiger E. Mitochondrial pathways and respiratory control an introduction to OXPHOS analysis. 2014 http://wiki.oroboros.at/images/f/fc/Gnaiger_2014_Mitochondr_Physiol_Network_MitoPathways.pdf

Gnaiger E, Kuznetsov AV, Schneeberger S, Seiler R, Brandacher G, Steurer W, et al. Mitochondria in the cold. Life Cold. 2000;431–42. https://doi.org/10.1007/978-3-662-04162-8_45

Gowers R, Linke M, Barnoud J, Reddy TJE, Melo MN, Seyler SL, et al. MDAnalysis: a python package for the rapid analysis of molecular dynamics simulations. Proc 15th Python Sci Conf. 2016; (Scipy; 98–105. https://doi.org/10.25080/majora-629e541a-00e

Guvench O. Revealing the mechanisms of protein disorder and N-glycosylation in CD44-hyaluronan binding using molecular simulation. Front Immunol. 2015;6:1–9. https://doi.org/10.3389/fimmu.2015.00305

Hales CN. The pathogenesis of NIDDM. Diabetologia. 1994;37-(Suppl 2):318–68. https://doi.org/10.1007/BF00400840

Krabbendam IE, Honrath B, Dilberger B, Iannetti EF, Branicky RS, Meyer T, et al. SK channel-mediated metabolic escape to glycolysis inhibits ferroptosis and supports stress resistance in C. elegans. Cell Death Dis. 2020;11:263. https://doi.org/10.1038/s41419-020-2458-4

Kruithof PD, Lunev S, Aguilar Lozano SP, de Assis Batista F, al-dahmani ZM, Joles JA, et al. Unraveling the role of thiosulfate sulfurtransferase in metabolic diseases. Biochim Biophys Acta Mol Basis Dis. 2020;1866(6):165716. https://doi.org/10.1016/j.bbadis.2020.165716

Kumari R, Kumar R, Lynn A. G-mmpbsa—a GROMACS tool for high-throughput MM-PBSA calculations. J Chem Inf Model. 2014;54(7):1951–62. https://doi.org/10.1021/ci500020m

Laskowski RA, MacArthur MW, Moss DS, Thornton JM. PROCHECK: a program to check the stereochemical quality of protein structures. J Appl Cryst. 1993;26(2):283–91. https://doi.org/10.1107/s0021889892009944

Le Guilloux V, Schmidtke P, Tuffery P. Fpocket: an open source platform for ligand pocket detection. BMC Bioinform. 2009;10:1–11. https://doi.org/10.1186/1471-2105-10-168

Leskovac V. Comperhansive enzyme kinetics. 1979; (Chapter 6: 111-116). Springer New York, NY.

Libiad M, Motl N, Akey DL, Sakamoto N, Fearon ER, Smith JL, et al. Thiosulfate sulfurtransferase-like domain-containing 1 protein interacts with thioredoxin. J Biol Chem. 2018;293(8):2675–86. https://doi.org/10.1074/jbc.RA117.000826

Liu N, Xu Z. Using LeDock as a docking tool for computational drug design. IOP Conf Ser Earth Environ Sci. 2019;218(1):012143. https://doi.org/10.1088/1755-1315/218/1/012143

Miller DM, Delgado R, Chirgwin JM, Hardies SC, Horowitz PM. Expression of cloned bovine adrenal rhodanese. J Biol Chem. 1991;266(8):4686–91. https://doi.org/10.1016/s0021-9258(19)67703-3

Moreno AJR. AngelRuizMoreno/Jupyter_Dock: v0.2.5. 2021 https://doi.org/10.5281/zenodo.5514956

Morton NM, Beltram J, Carter RN, Michailidou Z, Gorjanc G, McFadden C, et al. Genetic identification of thiosulfate sulfurtransferase as an adipocyte-expressed antidiabetic target in mice selected for leanness. Nat Med. 2016;22(7):771–9. https://doi.org/10.1038/nm.4115

Rao AA, Tayaru NM, Thota H, Changalasetty SB, Thota LS, Gedela S. Bioinformatic analysis of functional proteins involved in obesity associated with diabetes. Int J Biomed Sci. 2008;4(1):70–3.

Rosenbusch KE, Oun A, Sanislav O, Lay ST, Keizer-Gunnink I, Annesley SJ, et al. A conserved role for LRRK2 and Roco proteins in the regulation of mitochondrial activity. Front Cell Dev Biol. 2021;9:1–14. https://doi.org/10.3389/fcell.2021.734554

Salentin S, Schreiber S, Haupt VJ, Adasme MF, Schroeder M. PLIP: fully automated protein-ligand interaction profiler. Nucleic Acids Res. 2015;43(W1):W443–7. https://doi.org/10.1093/nar/gkv315

Selles B, Moseler A, Rouhier N, Couturier J. Rhodanese domain-containing sulfurtransferases: multifaceted proteins involved in sulfur trafficking in plants. J Exp Bot. 2019;70(16):4139–54. https://doi.org/10.1093/jxb/erz213

Smirnov A, Comte C, Mager-Heckel AM, Addis V, Krasheninnikov IA, Martin RP, et al. Mitochondrial enzyme rhodanese is essential for 5 S ribosomal RNA import into human mitochondria. J Biol Chem. 2010;285(40):30792–803. https://doi.org/10.1074/jbc.M110.151183

Sörbo BH, Lagerkvist U, Pesola R, Virtanen AI, Sörensen NA, Crystalline Rhodanese. II. The enzyme catalyzed reaction. Acta Chem Scand. 1953;7:1137–45. https://doi.org/10.3891/acta.chem.scand.07-1137

Sylvester DM, Sander C. Immunohistochemical localization of rhodanese. Histochem J. 1990;22(4):197–200. https://doi.org/10.1007/BF02386005

Wang Z, Sun H, Yao X, Li D, Xu L, Li Y, et al. Comprehensive evaluation of ten docking programs on a diverse set of protein-ligand complexes: the prediction accuracy of sampling power and scoring power. Phys Chem Chem Phys. 2016;18(18):12964–75. https://doi.org/10.1039/c6cp01555g

Wisastra R, Kok PAM, Eleftheriadis N, Baumgartner MP, Camacho CJ, Haisma HJ, et al. Discovery of a novel activator of 5-lipoxygenase from an anacardic acid derived compound collection. Bioorganic Med Chem. 2013;21(24):7763–78. https://doi.org/10.1016/j.bmc.2013.10.015

Xu D, Zhang Y. Improving the physical realism and structural accuracy of protein models by a two-step atomic-level energy minimization. Biophys J. 2011;101(10):2525–34. https://doi.org/10.1016/j.bpj.2011.10.024

SUPPORTING INFORMATION

Additional supporting information can be found online in the Supporting Information section at the end of this article.